Journal of
Composites Science

MDPI

Article

Structure and Dielectric Properties of Electroactive Tetraaniline Grafted Non-Polar Elastomers

Christopher Ellingford, Atcharaporn Pengchaicharoen, Alan M. Wemyss and Chaoying Wan *

International Institute for Nanocomposites Manufacturing (IINM), WMG, University of Warwick, Coventry CV4 7AL, UK; C.Ellingford@warwick.ac.uk (C.E.); atcharpe@scg.com (A.P.); A.Wemyss@warwick.ac.uk (A.M.W.)
* Correspondence: Chaoying.wan@warwick.ac.uk

Received: 28 February 2020; Accepted: 7 March 2020; Published: 10 March 2020

Abstract: Intrinsic modification of polybutadiene and block copolymer styrene–butadiene–styrene with the electrically conducting emeraldine salt of tetraaniline (TANI) via a three-step grafting method, is reported in this work. Whilst the TANI oligomer grafted at a similar rate to both polybutadiene and styrene–butadiene–styrene under the same conditions, the resulting elastomers exhibited vastly different properties. 1 mol% TANI-PB exhibited an increased relative permittivity of 5.9, and a high strain at break of 156%, whilst 25 mol% TANI-SBS demonstrated a relative permittivity of 6.2 and a strain at break of 186%. The difference in the behaviour of the two polymers was due to the compatibilisation of TANI by styrene in SBS through π-π stacking, which prevented the formation of a conducting TANI network in SBS at. Without the styrene group, TANI-PB formed a phase separated structure with high levels of TANI grafting. Overall, it was concluded that the polymer chain structure, the morphology of the modified elastomers, and the degree of grafting of TANI, had the greatest effect on the mechanical and dielectric properties of the resultant elastomers. This work paves the way for an alternative approach to the extrinsic incorporation of conducting groups into unsaturated elastomers, and demonstrates dielectric elastomers with enhanced electrical properties for use in actuation devices and energy harvesting applications.

Keywords: tetraaniline; SBS; polybutadiene; dielectric elastomer; intrinsic modification; relative permittivity; grafting; electroactive; electromechanical; actuation

1. Introduction

The ability to convert electrical energy to mechanical energy, or vice versa, is under extensive research due to a large array of applications. Smart electroactive polymers can change their shape through energy transduction from an electric field owing to Maxwell's stress, and can be applied to artificial muscle applications [1]. Alternatively, they can convert mechanical energy into electrical energy, resulting in energy harvesting. As an example, waste mechanical energy from transportation vehicle vibrations can be collected and utilised to power lighting and sensors. With the same mechanism, the conversion of mechanical energy from footsteps on a smart running track to power street lights is another challenging idea [2–6].

Electroactive materials require outstanding electromechanical properties. In the case of mechanical properties, the material should have a high strain at break, above 200%. In the case of electrical properties, the material should have the ability to store energy under an electric field, which can be described by the capacitance (*C*) and electrical energy density at breakdown (U_{el}) [7,8].

$$C = \varepsilon_r \varepsilon_0 \cdot \frac{A}{d} \quad (1)$$

$$U_{el} = 0.5CV^2 = 0.5\varepsilon_r\varepsilon_0 AdE_b^2 \quad (2)$$

Here, C is the capacitance of a parallel plate capacitor, A is surface area, d is thickness, V is applied voltage, ε_r is relative permittivity, ε_0 is permittivity of free space and E_b is electrical breakdown strength. Improvements in relative permittivity and electrical breakdown strength enhance the performance of energy harvesters [9–11] and actuators [4,12]. Therefore, the main electromechanical properties required of a dielectric elastomer are high relative permittivity and high electrical breakdown strength (> 50 V μm^{-1}) [10], while maintaining a high strain at break and a low dielectric loss, compared with relative permittivity (tan δ).

Dielectric elastomers are considered as electroactive polymers that produce large strains (200%–400%), large energy densities (10–150 kJ m^{-3}), low noise, light weight and fast response (10^{-3} s). However, electrical properties, such as relative permittivity, electrical breakdown strength and dielectric loss, must be improved to enhance their electromechanical properties. Therefore, a polar or a conducting filler can be introduced to enhance the electrical properties. To maximise the efficiency of a dielectric elastomer, the approach (intrinsic or extrinsic), the type of filler (high-permittivity nanoparticles or electrically conducting nanoparticles) and the concentration of the filler need to be considered carefully.

A high-permittivity conducting material can be introduced into a polymer by either extrinsic or intrinsic approaches. However, extrinsic mixing introduces issues with dispersion and agglomeration, owing to a poor compatibility between the filler and the polymer matrix. As a result, this degrades the mechanical properties and electrical breakdown strength, and results in a high tan δ, owing to interfacial defects [1–3,13]. On the other hand, the intrinsic approach can be achieved by many methods, such as hydrosilylation and thiol-ene click chemistry, and result in better compatibility and dispersity. Hydrosilylation allows a wide range of modifications, because a silicone-based polymer is grafted by a vinyl-terminated group. Thiol-ene click chemistry utilises an unsaturated polymer backbone, such as PVMS and SBS, to graft thiol groups and requires a short reaction time, minimal purification, and has a high product yield. However, thiols typically have a strong odour, reducing their practicality for a commercial product. Furthermore, chemical modification increases the dipole moment across the polymer chain (permanent polarity), while maintaining a low *tan* δ. The electrical breakdown strength of this homogeneous polymer is enhanced while maintaining the deformable nature of the polymer matrix [14–16].

We next consider the types of conducting groups that can be grafted to a polymer backbone, namely: (1) nanoparticles with high permittivity, such as $BaTiO_3$, PZT and TiO_2, or (2) high-electrical-conductivity nanoparticles, such as carbon nanotubes (CNTs), graphene and metallic fillers. Stoyanov et al. grafted polyaniline (PANI) to a poly-styrene-co-ethylene-co-butadiene-co-styrene-g-maleic anhydride (SEBS-g-MA) elastomer [1]. They found that the permittivity of the grafted material increased to up to 470% relative to that of the polymer matrix, while maintaining the electrical breakdown strength. However, the long-chain PANI caused the distant migration of the charge on the backbone, resulting in a high tan δ [17–22].

TANI is a short π-conjugated oligomer of aniline containing four aniline units. Owing to its short length, the main properties of this oligo(aniline) are good solubility and excellent processability compared with PANI. TANI has multiple different oxidation states, however the emeraldine-based state is the most desirable form, as it can be acidified to form the emeraldine salt (ES) state resulting in high conductivity (approximately 0.014 S m^{-1}) [23]. As TANI is one of the most outstanding organic semiconductors that can be potentially used for many purposes, it represents an excellent high-permittivity conducting material [24–26].

With low grafting, the relative permittivity of the elastomer slowly increases because the conducting particles are dispersed far from each other in the polymer matrix. Adding conducting particles until a particular point wherein the conducting clusters are located very close together, but are separated by a very thin elastomer matrix layer, results in the formation of microcapacitors. A high degree of microcapacitors enhances the relative permittivity and capacitance of the composite signficantly.

However, if the loading content is too high, the percolation threshold will be research and the permittivity of the material will decrease.

Thus, permittivity can be significantly improved by adding conducting particles until just before the percolation threshold is reached [21,27–31].

In this research, poly(styrene-butadiene-styrene) (SBS) and polybutadiene (PB) were studied as elastomer matrices. The backbone of the block copolymer SBS contains polystyrene and polybutadiene. The polystyrene block improves the durability and rigidity of SBS, whereas the polybutadiene block results in a soft and flexible behaviour. Moreover, this thermoplastic elastomer also shows a high strain at break (>800%), high electrical breakdown strength (approximately 65 V μm^{-1}) and low tan δ (0.01) [2,32]. On the other hand, polybutadiene (PB) has no styrenic component, making the material softer than SBS (2400% strain at break), and have a low tan δ (0.01). Owing to their high strain and different components on the backbone [33–37], SBS and PB were chosen for this study.

In this study, a thermoplastic elastomer SBS was modified by intrinsic modification with π-conjugated conducting emeraldine salt TANI (ES-TANI) to enhance its polarity and electromechanical properties. The intra- and intermolecular interactions between the pedant TANI groups and the backbone were analysed through the characterisation of the microstructure and mechanical and electrical properties. TANI-grafted PB was synthesised to illustrate the role of the polymer backbone in the electromechanical properties.

2. Materials and Methods

2.1. Materials

N-Phenyl-*p*-phenylenediamine (98%), ammonium persulophate (APS, 98%), toluene (99%), formic acid (95%), hydrogen peroxide (30%) and trifluoroacetic acid (99%) were purchased from Sigma-Aldrich (Schnelldorf, Germany). Ammonium hydroxide (Acros Organics, 30%), hydrochloric acid (HCl, 37%) and acetone (99%) were purchased from Fisher Scientific (Loughborough, UK). Poly(styrene-butadiene-styrene) block copolymer (SBS, Vector 8508A) was purchased from Dexco (Taipei City, Taiwan R.O.C.). PB (96% cis 1,4 content, BUNA CB 24) was purchased from Arlanxeo (Maastricht, The Netherlands). Tetrahydrofuran (THF, GPR Rectapur, 99.9%) was purchased from VWR (Lutterworth, UK). Carbon conductive grease used as a compliant electrode for electrochemical impedance spectroscopy (EIS) studies was purchased from MG Chemicals (Surrey, BC, USA). All chemicals were used as received.

2.2. Synthesis of Tetraaniline (TANI) [38]

N-phenyl-*p*-phenylenediamine (18.525 g, 0.10 mol) was dissolved in 150 mL of acetone at 0 °C in an ice bath. Then 100 mL of 1 M HCl solution was added. Meanwhile, 45.636 g (0.2 mol) of APS was dissolved in 80 mL of 1 M HCl, and gradually added to the N-phenyl-*p*-phenylenediamine solution using a double syringe pump at a feed rate of 4 mL/min. After the feeding, the solution was continuously stirred vigorously at room temperature for 1.5 h. The crude product was filtered and washed by adding 30 mL of the 1 M HCl followed by 80 mL of water. The dried sample was dispersed in 1 L of a 1 M ammonium hydroxide solution, and allowed to react for 2 h. The product was then again filtered and washed with DI water. Finally, the sample was dried in a vacuum oven for 48 h. ^{1}H-NMR (400 MHz, $CDCl_3$): δ = 7.52 (br, 1 H, $H_{benzene}$), 7.37 (br, 2 H, $H_{benzene}$), 7.00 (br, 2 H, $H_{benzene}$), 6.94 (br, 1 H, $H_{benzene}$), 3.75 (br, 2 H, NH_2) ppm. FTIR (cm^{-1}): 3367, 3192, 1598, 1579, 1513, 1495, 1307, 1155, 818, 748, 694

2.3. Synthesis of TANI-SBS

For the epoxidation of SBS, 3 g of SBS was dissolved in 27 g of toluene at room temperature for 0.5 h. Formic acid and hydrogen peroxide were gradually added to the stirred solution in accordance with the desired grafting ratio (mol%). Then the solution was allowed to react for 4 h at 60 °C to

make epoxidised SBS (E-SBS). Following this, the E-SBS was precipitated in methanol and dried in air for 1.5–2 h. E-SBS was then dissolved in 50 mL of THF, followed by the addition of TANI, and the solution was continuously stirred until the TANI dissolved. Then the reaction was allowed to continue overnight at 60 °C.

The TANI was acidified to the emeraldine salt oxidation state to enhance conductivity by adding trifluoroacetic acid and was allowed to react at room temperature for 5 h. Finally, TANI-SBS was purified by two steps. First, the solution was directly filtered under vacuum to remove the excess acidified TANI. The acidified TANI-SBS remained in solution. Secondly, the TANI-SBS solution was precipitated by stirring in methanol and dried in a vacuum oven at 40 °C overnight. ^{1}H NMR (400 MHz, $CDCl_3$): δ = 7.10 (br, 3 H, $H_{benzene}$), 6.62 (br, 2 H, $H_{benzene}$), 5.45 (br, 4 H, –HC=C**H**– and –HC=C**H**$_2$), 5.01 (br, 1 H, –**H**C=CH$_2$), 4.42 (br, 1 H, –(CH$_2$)(CHOH)C**H**NH–), 2.96 (br, 1 H, C**H**OH), 2.72 (br, 1 H, –CH–O–C**H**–), 2.11 (br, 1 H, (–H$_2$C)$_2$C**H**CH–), 2.07 (br, 3 H, (–H$_2$C)$_2$C**H**CH$_{benzene}$ and –CH$_2$C**H**$_2$CH–), 1.61 (br, 2 H, (H$_2$C)$_2$C**H**$_2$), 1.45 (br, 2 H, (CH)$_2$C**H**$_2$) ppm. ^{13}C NMR (75 MHz, $CDCl_3$): δ = 129.07 (H**C**=CH and HC=**C**H$_2$), 125.33 ($C_{benzene}$), 114.80 (H**C**=CH$_2$), 65.54 –(CH$_2$)(CHOH)**C**HNH–), 58.54 (–**C**HOH–), 32.75 (–H$_2$C)$_2$**C**H– and –H$_2$C**C**H$_2$CH–), 27.43 ((–H$_2$C)$_2$**C**HCH–) ppm. FTIR (cm^{-1}): 3262, 2918, 2967, 1781, 1672, 1667, 1493, 1302.

2.4. Synthesis of TANI-PB

For the epoxidation step of PB, 3 g of PB was dissolved in 80 g of toluene at room temperature for 3 h. Formic acid and hydrogen peroxide were gradually added to the stirred solution in accordance with the desired grafting ratio (mol%). Then the solution was allowed to react for 4 h at 60 °C to make epoxidised-PB (E-PB). When the reaction ended, E-PB was precipitated in methanol and dried in air for 1.5–2 h. Then it was subsequently dissolved in 50 mL of THF (approximately 1 h). TANI was added and the solution was continuously stirred until the TANI dissolved to make grafted TANI-PB and the reaction was allowed to continue overnight at 60 °C. TANI-PB was acidified by adding trifluoroacetic acid and allowed to react at room temperature for 5 h. Finally, TANI-PB was purified by the same two steps used in the case of TANI-SBS. First, the solution was directly filtered under vacuum to remove the excess acidified TANI. The acidified TANI-PB remained in solution. Secondly, the TANI-PB solution was precipitated by stirring in methanol, and dried in a vacuum oven at 40 °C overnight. ^{1}H NMR (400 MHz, $CDCl_3$): δ = 5.42 (br, 2 H, –HC=C**H**–), 4.38 (br, 1 H, –(CH$_2$)(CHOH)C**H**NH–), 2.74 (br, 1 H, C**H**OH) ppm. FTIR (cm^{-1}): 3253, 3068, 3003, 2919, 1672, 1572, 1505, 1370.

2.5. Characterisation

For ^{1}H NMR and ^{13}C NMR, all data was obtained using a Bruker AVANCE III HD 400 MHz spectrometer. Chemical shifts were internally referenced to TMS using chloroform-*d* ($CDCl_3$). The spectra were analysed using ACD/NMR processor version 12.01 (ACD/Labs). Fourier transform infrared (FTIR) spectroscopy results were obtained with 32 scans at a resolution of 4 cm^{-1} using Bruker TENSOR 27. Gel permeation chromatography (GPC) was performed using Agilent 390-MDS with two PLgel mixed-C columns and THF as an eluent (pressure 77–79 bar, flow rate 1 mL/min) and analysed using Agilent GPC/SCE software. For impedance spectroscopy, the samples (thickness = 100–200 µm) were prepared by Rondol manual compression moulding at 190 °C. Carbon black grease was applied onto both sides of the compressed surface to act as a compliant electrode. Electrical properties were measured from 10^0 to 10^6 Hz using a Princeton Applied Research Parastat MC with a PMC-2000 card and a two-point probe. Mechanical testing samples were prepared following the ASTM-D638-14 type V standard. The experiments were carried out using a Shimadzu Autograph AGS-X tester at room temperature with a 50 mm min^{-1} extension rate and a 0.1095 s^{-1} strain rate (10 kN load cell). Samples (size 5.0 mm × 5.0 mm × 2.3 mm) were analysed by dynamic mechanical thermal analysis (DMTA) from −120 to 135 °C in the single-cantilever mode with a frequency of 1 Hz and an amplitude of 50 µm. Scanning electron microscopy (SEM) samples were prepared by cryo-fracturing in liquid nitrogen. The fractures were placed onto carbon tape and sputter-coated with Au/ Pd. SEM images were obtained

with a CARL ZEISS: MERLIN™ field emission scanning electron microscope. For UV-vis spectroscopy, the diluted samples were prepared by dissolving in dichloromethane (DCM) to a concentration of 1×10^{-5} mol dm^{-3}. All samples were analysed using an Agilent Cary 60 spectrophotometer between 200 and 800 nm.

3. Results and Discussion

The synthesis of tetraaniline (TANI) was characterised by Gel Permeation Chromatography (GPC), ^{1}H NMR and FTIR. The GPC trace in Figure S1 shows the formation of oligomeric aniline, with a number average molecular weight (M_n) of 648 g mol^{-1} and a polydispersity index (PDI) of 1.58. From the slightly high M_n and PDI, and the shape of the trace in Figure S1, the main product formed consists of four aniline units, accompanied by some higher order structures formed during the reaction, such as hexamers and octamers. These products are similar in nature and solubility to tetraaniline, making their removal challenging. Therefore, the conditions of the reaction were controlled to minimise octaaniline formation, including limiting the reaction time to 1.5 h. The resulting product was a dark blue colour, confirming that the oxidation state of TANI was emeraldine base [39].

^{1}H NMR in Figure S2 confirmed the structure of TANI. Peaks at 3.76 ppm and 7.39 ppm show two NH groups in emeraldine base TANI. The aromatic system of TANI is shown by the peaks at 7.10 ppm, 6.96 ppm, 5.80 ppm and 5.51 ppm. The results match well to previously reported TANI [23,40]. Furthermore, FTIR in Figure S3 confirms the presence of an N–H stretch at 3376 cm^{-1}, an aromatic C–H stretch at 2955 cm^{-1}, the quinoid of TANI ring at 1597 cm^{-1} and the benzoid ring of TANI at 1495 cm^{-1}. Overall, the combination of GPC, FTIR and ^{1}H NMR confirm the structure of TANI.

When TANI is converted to the emeraldine salt morphology, it can form a nanowire arrangement when acidified using acids such as HCl, due to the small counterion size of Cl. However, when acids with larger counterions are used, the nanowire structure is disrupted. For solubility in THF, trifluoroacetic acid was used to acidify TANI, and the large counterion size formed agglomerated TANI instead of a defined nanowire morphology formed, see Scheme 1.

The grafting of TANI to both SBS and PB was completed via a 3-step mechanism, as shown in Scheme 1. In the first step, the alkenes of SBS and PB are epoxidised using the molar equivalents of H_2O_2 and formic acid. The formation of epoxidised SBS (E-SBS) introduced two new peaks at 2.96 and 2.72 ppm in ^{1}H NMR in Figure 1, from the proton environments attached to the two carbons in the epoxide ring. In comparison, the epoxidation of PB formed one broad peak at 2.96 ppm. The grafting efficiency of the reaction was 50%, compared to the molar equivalents of formic acid and hydrogen peroxide used. It was also found that the solubility of E-SBS and E-PB deteriorated drastically at grafting ratios of 50% or higher.

E-SBS and E-PB were unstable products, and thus were reacted with TANI after two hours drying in air to prevent the epoxide rings of E-SBS and E-PB ring opening and crosslinking the polymer chains autonomously. The ring opening reaction between the primary amine at the ω-terminus of TANI and the epoxide rings achieved completion at an elevated temperature of 60 °C. After the ring opening reaction was complete, the grafted TANI was acidified with trifluoroacetic acid to convert TANI from the emeraldine base oxidation state to the emeraldine salt form. The resulting polymers were green in colour.

The confirmation of grafting TANI to SBS and PB came from ^{1}H NMR and FTIR in Figure 1 and Figures S3–S5. In TANI-SBS, the epoxide proton at 2.96 ppm shifted to 4.41 ppm as the NH_2 of TANI opened the ring. Furthermore, FTIR of TANI-SBS (Figure S3) confirms the presence of OH from a broad peak at 3300–3200 cm^{-1}, a C–N stretch at 1672 cm^{-1} and the presence of both the quinoid and benzoid ring at 1597 cm^{-1} and 1495 cm^{-1}, respectively.

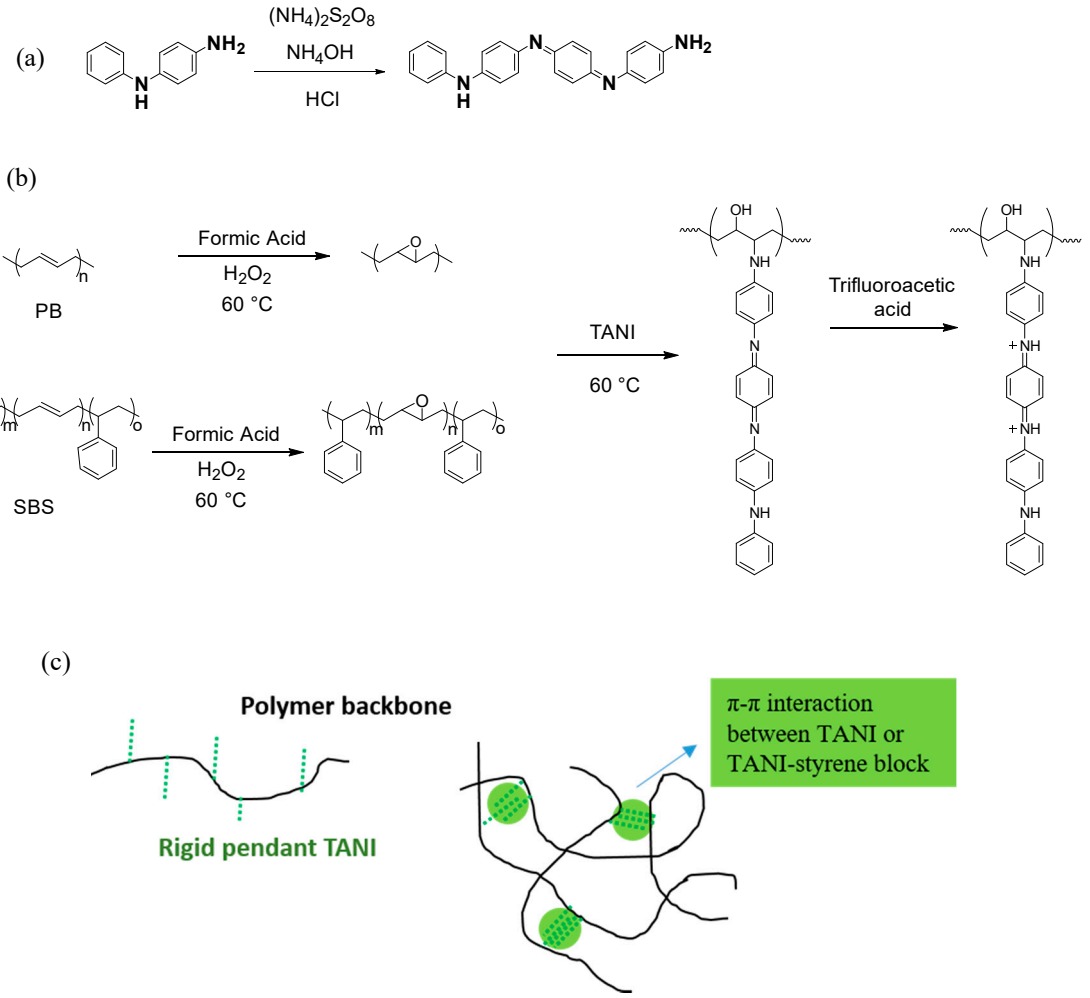

Scheme 1. (**a**) the synthesis of TANI in the emeraldine base oxidation state. (**b**) The grafting of TANI to both SBS and PB and the oxidation of grafted TANI to the emeraldine salt oxidation state. (**c**) Schematic diagram showing π-π stacking regions between TANI oligomers or TANI-PS.

Similarly, for TANI-PB, FTIR and ^{1}H NMR in also confirming the grafting of TANI. The peak at 2.96 ppm splits into two resolved singlets after the ring opening reaction at 2.94 and 3.01 ppm due to splitting of the proton environment from the combination of the hydroxyl group and TANI attachment. In addition, a peak at 4.38 ppm appears due to the attachment of TANI to the polymer backbone. The presence of the aromatic protons in TANI cannot be observed in either NMR for TANI-SBS and TANI-PB, as TANI is in the emeraldine salt oxidation state, which has limited solubility in most solvents, including $CDCl_3$. FTIR of TANI-PB shows the presence of an NH stretch at 3246 cm^{-1}, a C–N stretch at 1669 cm^{-1}, and the quinoid and benzoid rings of TANI at 1597 and 1495 cm^{-1}. From ^{1}H NMR, the grafting levels of TANI to SBS was 25 mol% and 35 mol% with respect to the butadiene backbone, and the grafting of TANI to PB was 1 mol%, 25 mol% and 35 mol%. This approach enabled the normally insoluble and unprocessable emeraldine salt TANI to be grafted to the polymer backbone, resulting in homogenous dispersion throughout the matrix for uniform electromechanical properties, as well as an elastomer which can be easily processed and solubilised. 50 mol%-grafted TANI-SBS and TANI-PB were also synthesised; however they yielded brittle, non-elastic products.

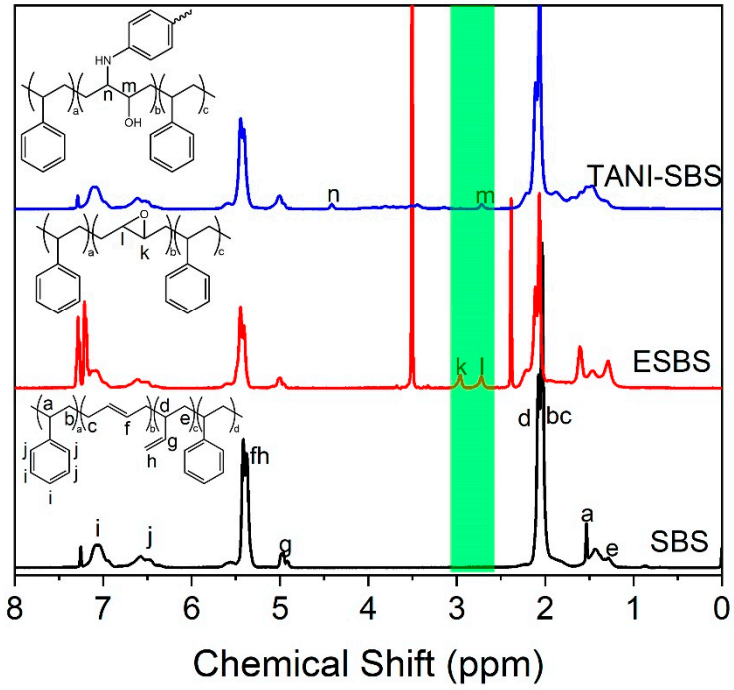

Figure 1. Protonic nuclear magnetic resonance (^{1}H NMR) spectra of styrene-butadiene-styrene (SBS), epoxidised SBS (ESBS) and TANI-SBS.

The effect of grafting of TANI on the physical behaviour of the elastomers is observed in DMTA, Figure 2. Using SBS as an example, the glass transition temperature shifts to higher temperatures upon higher grafting. In SBS, there are two glass transition temperatures, at −83 °C and 97 °C. These are attributed to the soft butadiene block and the hard styrene block, respectively. Upon grafting 25 mol% of TANI to the butadiene block, three glass transition temperatures are observed at −52 °C, −15 °C and 76 °C. These are attributed to the partially modified butadiene backbone, which had an increase in glass temperature due to the loss of flexibility, the TANI groups and the styrene block, respectively. As the TANI grafting increased to 35 mol% and 50 mol%, the glass transition peak for the modified butadiene chain disappeared, and the glass transition from TANI become dominant in the properties of the polymer. At 50 mol%, TANI-SBS has a glass transition temperature of 46 °C for TANI and 88 °C for the styrene block. This explains the brittleness of the modified polymer, as 50 mol% TANI-SBS is in a glass state at room temperature. Figure S6 shows that this is the reason for the brittleness of 50 mol% TANI-PB as well.

To further understand the behaviour observed in DMTA, the intrinsic interactions from TANI were investigated using UV-Vis spectroscopy. In Figure S7, the UV-Vis spectra of TANI shows that there are three defined transition peaks. At 299 nm there is the benzoid transition from the π-π^* transition on the ring, at 416 nm the quinoid (polaron) transition from the emeraldine salt oxidation state of TANI, and finally the bipolaron (exiton) transition between 700–800 nm located on the quinoid ring. This transition arises due to electron donation from the adjacent benzoid rings [41,42].

After grafting 25 mol% TANI to SBS, the benzoid and quinoid transition of TANI red-shifted and the smooth bipolaron transition disappears, leaving some sharper transition peaks remaining in the region of 600–800 nm. In addition, the π-π* transition for styrene on SBS remained unchanged. SBS is a block copolymer with a phase separated structure, and this demonstrated that the aromatic region of SBS is unaffected. The red shift indicates that it requires less energy to promote an electron in the quinoid and benzoid transitions for TANI, and suggests that TANI only π-π stacks between TANI oligomers at 25 mol% grafting, creating an electron-rich environment. It indicates that the butadiene block and styrene block maintain a phase separated morphology and explains the presence of three glass transition temperature peaks for 25 mol% TANI-SBS in Figure 2.

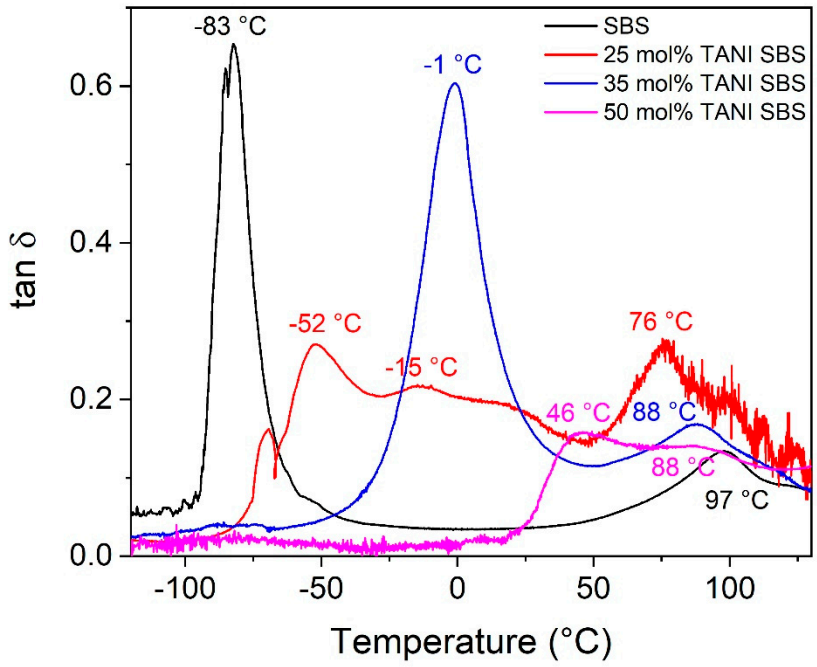

Figure 2. Dynamic mechanical thermal analysis (DMTA) tan δ for the T_g of SBS, 25 mol% TANI-SBS, 35 mol% TANI-SBS and 50 mol% TANI-SBS.

However, the UV-Vis spectroscopy behaviour of 35 mol% TANI-SBS is somewhat different. The bipolaron region and π-π^* benzoid transition blue shifts to between 550–700 nm and to 291 nm, respectively. Furthermore, the π-π^* transition for the styrenic block of SBS also blue shifts, but the quinoid transition remains identical to TANI. The blue shift of the bipolaron region indicates that less electron density from adjacent benzoid rings is being shared with the quinoid ring. Furthermore, the blue shift of both the benzoid ring and the styrenic block indicates that the two regions are interacting through π-π stacking, despite the phase-separated structure of SBS. This indicates that the grafting of TANI altered the phase morphology of the polymer, allowing the two groups to interact. Finally, as the quinoid transition is unaffected, it is not involved in this interaction. The dominating nature of TANI on the properties of the butadiene backbone explains the reduction in the number of glass transition peaks from three to two upon an increase in grafting.

In 25 mol% TANI-PB, the electron rich environment present in TANI SBS does not appear in PB, and the benzoid and quinoid transitions of TANI do not shift wavelength. However, the bipolaron transition splits into two broad peaks between 500–600 nm and 700–800 nm. Additionally, the π-π^* alkene transition in TANI-PB is not observable due to the strong benzoid transition. As the peaks do not shift, it indicates that there is less TANI π-π stacking in 25 mol% TANI-PB—at least in the solution state. This is attributed to the longer chains of PB, as noted in the GPC of both SBS and PB in Figure S8, whereby SBS has a $M_w \approx 100{,}000$ g mol^{-1} and PB has a $M_w \approx 600{,}000$ g mol^{-1}, meaning that the grafting density of TANI is lower in PB than in SBS.

In 1 mol% TANI-PB, the transitions attributed to TANI are not visible due to the low content of grafted TANI. However, the π-π^* transition is visible at 276 nm from the alkenes of PB, and is broader than in PB due to the benzoid transition acting as a shoulder peak. The solubility of 35 mol% TANI-PB was too low to obtain UV-Vis results.

SEM imaging, as seen in Figure 4, demonstrated the observable differences in the polymer morphology of both PB and SBS as the grafting of TANI is increased. Figure 4a–c shows how the morphology of SBS changes between 25 mol%, 35 mol% and 50 mol% grafting. At 25 mol% grafting, there is a phase separated structure between the butadiene dominating TANI-butadiene block and the styrene block. At 35 mol% grafting, the morphology changes to show a more compatibilised polymer morphology, as two distinct polymer phases are not observable. However, at 50 mol% grafting,

two distinct polymer phases are observed once more, the TANI-dominated butadiene block and the styrene block, confirming the observations from DMTA and UV-Vis spectroscopy in Figures 2 and 3. In Figure 4d,e, TANI-PB with both 25 mol% and 50 mol% grafting showed a phase separated morphology, attributed to the lack of compatibilisation between the TANI and butadiene chains and resulting in TANI/butadiene phase separation

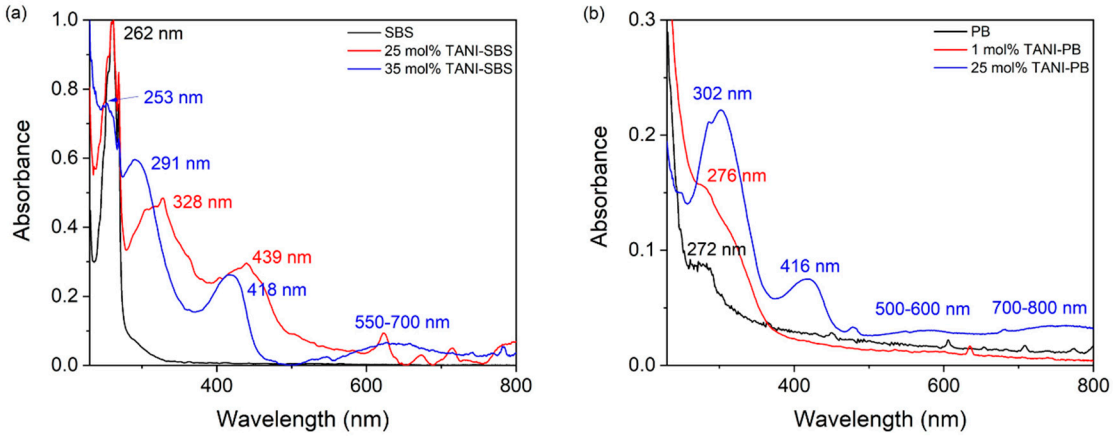

Figure 3. (**a**) UV-Vis spectroscopy of SBS, 25 mol% TANI-SBS and 35 mol% TANI SBS. (**b**) UV-Vis spectroscopy of PB, 1 mol% TANI-PB and 25 mol% TANI-PB.

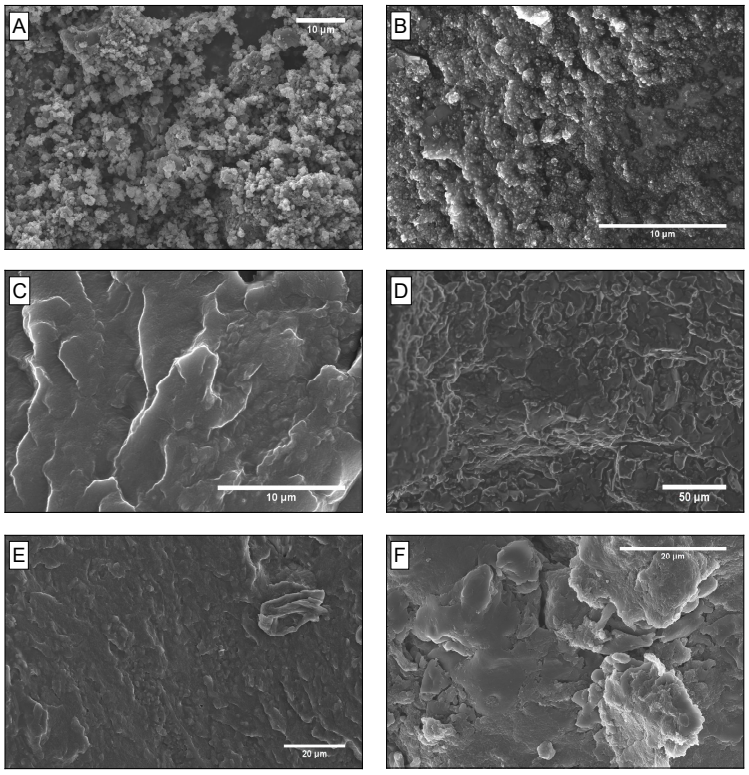

Figure 4. SEM imaging of the cryo-fractured surface of (**A**) TANI in the emeraldine salt oxidation state (**B**) 25 mol% TANI-SBS, (**C**) 35 mol% TANI SBS, (**D**) 50 mol% TANI-SBS, (**E**) 25 mol% TANI-PB and (**F**) 50 mol% TANI-PB.

Tensile testing of the TANI-grafted elastomers revealed that the mechanical properties are highly dependent on the TANI grafting ratio, as seen in Figure 5. Prior to modification, SBS and PB had a strain at break of 857% and 2442%, and a tensile strength of 8.92 MPa and 0.15 Mpa, respectively, see Figure S9. After grafting, the tensile strength of 25 mol% TANI-SBS reduced significantly to 2.93 MPa

and the strain at break decreased to 186%. The decrease in the strain at break is due the grafting of a 'hard' TANI block, which behaves similarly to the styrenic block and reduces the flexibility of the 'soft' butadiene block, whereas the tensile strength decreased due to the phase-separated nature. Additional increases in the TANI grafting to form 35 mol% TANI-SBS demonstrated only a small further decrease in the strain at break to 167%, but a large increase in the tensile strength to 8.71 MPa. The large increase in the tensile strength is attributed to the change in phase morphology observed in UV-Vis, DMTA and SEM imaging in Figures 2–4. The morphology changes as the TANI groups π-π stack with the styrenic block, increasing the interchain strength. Despite the morphology change, the strain at break decreases further due to the increase of the 'hard' TANI groups reducing the flexibility of the 'soft' butadiene chain. Finally, 50 mol% TANI-SBS could not be tested due to its brittleness. This was due to phase separation between the TANI-butadiene and styrene block and the high T_g of the polymer.

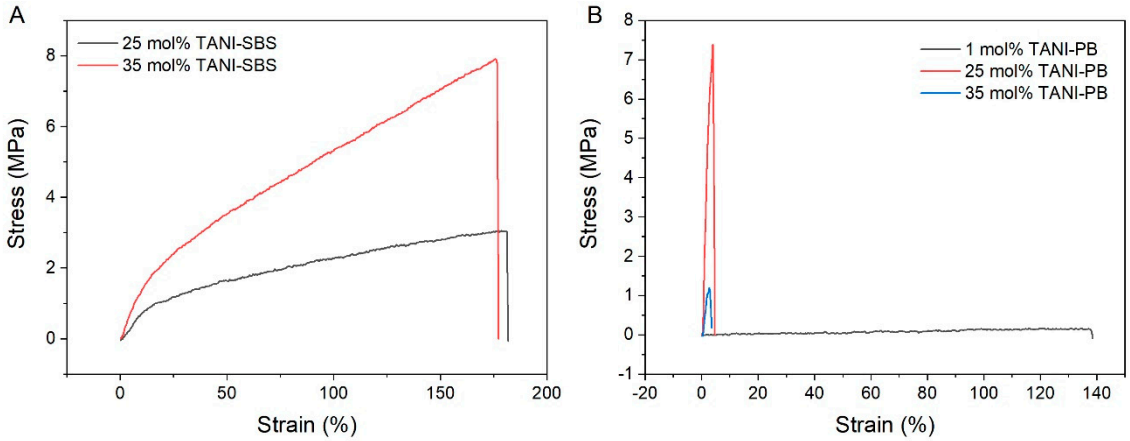

Figure 5. Stress–strain curves for (**A**) 25 mol% TANI SBS, 35 mol% TANI-SBS, and (**B**) 1 mol% TANI-PB, 25 mol% TANI-PB, 35 mol% TANI-PB.

Comparatively, grafting both 25 mol% and 35 mol% TANI to PB resulted in brittle products with a very low strain at break of 4%–5%, down from 2442%. This was attributed to the lack of compatibility between grafted TANI and PB, from the phase separation observed in SEM imaging in Figure 4. The difference in behaviour between TANI-modified SBS and PB polymers is due to the compatibilisation of TANI from the styrene block of SBS through π-π stacking.

Therefore, to increase the elongation at break for TANI-PB, a reduction in the grafting was required. To achieve this, 1 mol% TANI-PB was synthesised to retain the flexibility of the butadiene chain, and to reduce the phase separation observed. 1 mol% TANI-PB demonstrated a strain at break of 156% and a tensile strength of 0.22 MPa.

Thus overall, the grafting of TANI to SBS yielded materials with the highest strain at break and largest tensile strength, making them suitable for actuation and energy harvesting devices.

Impedance spectroscopy of emeraldine salt TANI in Figure S10 shows a conducting material with an ac conductivity of 1.4×10^{-2} S m^{-1} at 10^3 Hz, with only a small observable frequency dependence. The phase angle for the material was 0° between 10^0 Hz and 10^4 Hz, demonstrating the conducting nature of TANI. In addition, the relative permittivity of TANI was 3189 at 10^3 Hz accompanied by a high tan δ loss of 77.8 at 10^3 Hz (where $\tan\delta = \frac{dielectric\ loss}{relative\ permittivity}$). Thus, the conducting nature of TANI represents an ideal group to introduce as a series of microcapacitors by grafting onto SBS and PB to enhance their relative permittivity.

Figure 6a shows that the relative permittivity of 25 mol% TANI-SBS was enhanced to $\varepsilon_r \approx 6.2$ at 10^3 Hz compared to $\varepsilon_r \approx 2.8$ at 10^3 Hz. The relative permittivity remains constant between 10^2–10^6 Hz, however below 10^2 Hz the relative permittivity increases significantly due to electrode polarisation. The relaxation peak for electrode polarisation is observed in both tan δ and phase angle at 10^1 Hz, in Figure 6c,e, respectively. Prior to the relaxation peak, 25 mol% TANI-SBS exhibits a low tan δ loss of

0.25 at 10^3 Hz and a phase angle of −90° to demonstrate its insulating nature, compared to 0.009 and −90° at 10^3 Hz for SBS, respectively.

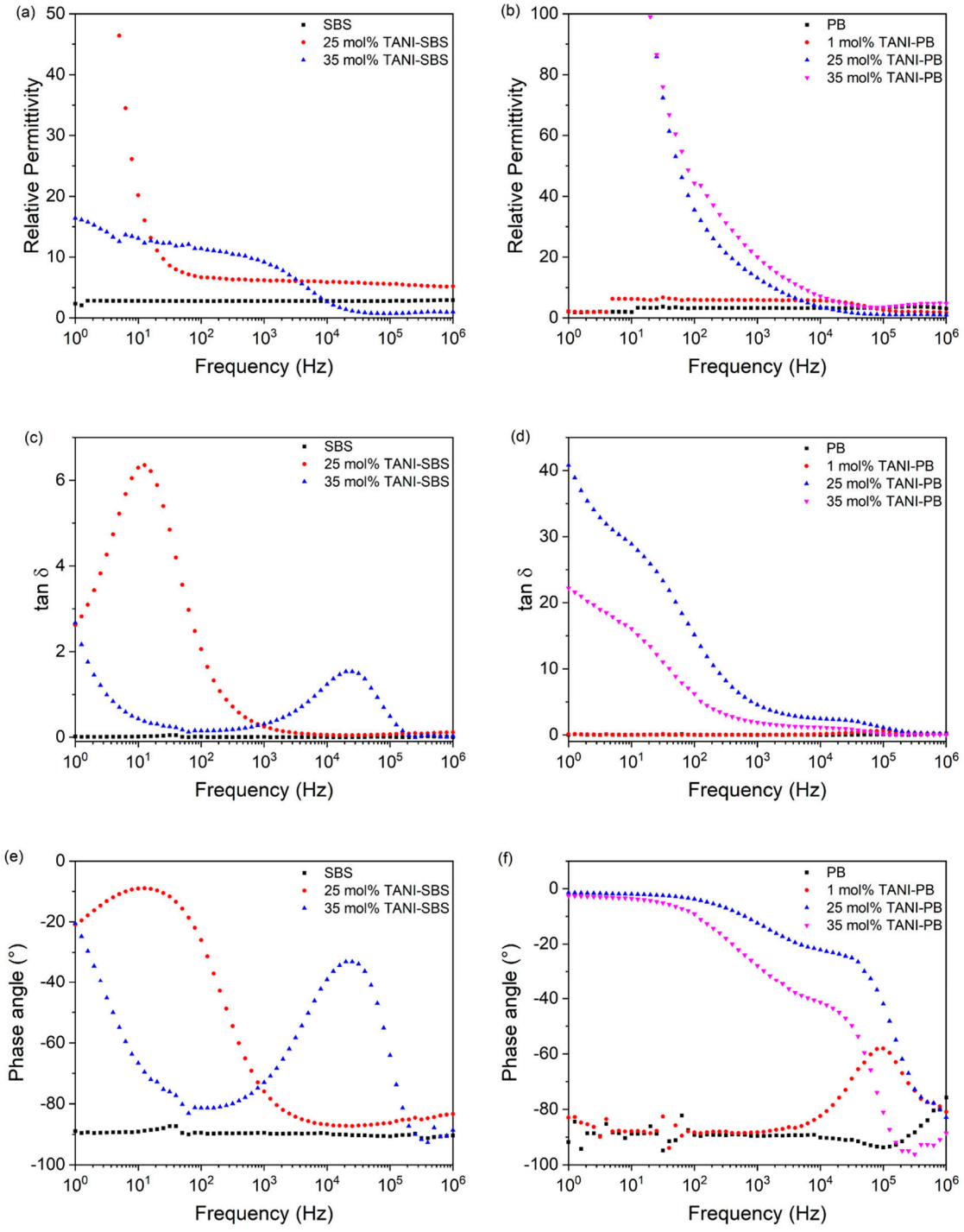

Figure 6. Dielectric properties of TANI modified SBS and PB.

Increasing the TANI grafting to 35 mol%, TANI-SBS enhanced the relative permittivity to 9.2 at 10^3 Hz. Due to the change in phase morphology exhibited in 35 mol% TANI-SBS, electrode polarisation was not observed at low frequency, as the increase in compatibilisation disrupts any conducting TANI network, ensuring grafted TANI maintains its micro-capacitor behaviour, and prevents electrons from building up at the electrodes. However, a decrease in the relative permittivity was observed at 10^4 Hz, attributed to molecular polarisation and the inability of TANI-butadiene to respond to the alternating

electric field. The molecular polarisation is also observed in tan δ and phase angle at 10^4 Hz as a relaxation peak. In addition, the tan δ of 35 mol% TANI-SBS was 0.31 at 10^3 Hz. Due to molecular polarisation peak, followed by the beginning of electrode polarisation at low frequency, the phase angle for 35 mol% TANI-SBS remains mostly deviated from −90°. Comparatively to literature examples, 35 mol% TANI-SBS demonstrates superior relative permittivity, and low tan δ loss compared to examples involving the conducting polymer form of TANI, polyaniline [1].

For PB, the relative permittivity was 3.3, and the tan δ was 0.009 at 10^3 Hz, as seen in Figure 6b,d. Additionally, the material was highly insulating with an ac conductivity of 1.5×10^{-9} S m^{-1} and a phase angle of −90° at 10^3 Hz, shown in Figure S11 and Figure 6f. Upon grafting of 1 mol% TANI to PB, the relative permittivity increased to 5.9 at 10^3 Hz. A reduction in the permittivity above 10^5 Hz was due to molecular polarisation.

Furthermore, the tan δ loss remained low at 0.03 at 10^3 Hz and showed a small relaxation peak at 10^5 Hz attributed to molecular polarisation. The phase angle of the polymer remains at −90° between 10^0–10^4 Hz to demonstrate that the incorporation of 1 mol% TANI does not introduce a conducting network into PB. However, the phase angle then deviates from −90° between 10^4–10^6 Hz due to molecular polarisation.

However, grafting both 25 mol% and 35 mol% TANI to PB resulted in the formation of a conducting TANI network in the elastomer due to phase separation between TANI and PB, observed in SEM imaging in Figure 4. The relative permittivity increases to 13.2 and 20.0 for 25 mol% TANI-PB and 35 mol% TANI-PB, respectively. Due to the conductive network, the relative permittivity increases to over 100 below 10^2 Hz. The conductive nature of these two elastomers is also observed by the high tan *d* loss experienced by both materials and a phase angle deviated away from −90°. The conducting nature of these materials is reinforced by the elevated conductivities of 3.3×10^{-6} S m^{-1} and 2.1×10^{-6} S m^{-1} for 25 mol% TANI-PB and 35 mol% TANI-PB, respectively. In these elastomers, the formed TANI network allows the conduction of electrons through it, instead of TANI behaving as microcapacitors.

4. Conclusions

In summary, using a three-step grafting procedure, TANI in the emeraldine salt form was successfully attached to the polymer backbones of SBS and PB with a view to enhance the relative permittivity of these elastomers. TANI was synthesised in the non-conductive emeraldine base form, before grafting to epoxidised SBS and PB through a ring opening reaction and acidification to the emeraldine salt form.

Different grafting ratios of TANI to SBS and PB were investigated, and it was found that 50 mol% grafting of TANI yielded an insoluble material with a poor strain at break. The reduction in the mechanical properties was due to the increase in glass transition temperature from an increased grafting of TANI, as the glass transition temperature for TANI is similar to styrene due to π-π stacking interactions. Thus, lower grafted TANI-SBS and TANI-PB retained their elastomeric behaviour and demonstrated a strain at break of up to 186% for 25 mol% TANI-SBS and a tensile strength of 2.9 MPa.

Further investigation into this behaviour through SEM imaging explained the effect of TANI on the mechanical properties for both SBS and PB. In PB, TANI and PB were incompatible with each other, and thus generated a phase separated morphology. In SBS, the styrenic block aided compatibilisation through π-π stacking, which retained the elastomeric properties of SBS up to 35 mol% TANI-SBS, demonstrating that the presence of a 'hard' block in SBS is essential.

The electrical properties of TANI-PB showed that only 1 mol% of TANI was required to enhance the relative permittivity of the elastomer significantly, from 3.3 to 5.9, whilst maintaining a low tan δ loss and an insulating behaviour. Increasing with further TANI grafting yielded a conductive polymer from a percolation network of TANI chains. In SBS, percolation is not observed until after 35 mol% grafting, which led to increases in the relative permittivity from 2.8 to 6.2 and 9.2 and 25 mol% and 35 mol% grafting, respectively. However, at 35 mol% grafting, the phase angle deviated away from −90° across all frequencies, indicating that the behaviour of the elastomer is no longer fully insulating

anymore. The compatibilisation between styrene and TANI disrupted the formation of a conducting TANI network, at this grafting level. The limitation for TANI-SBS is grafting over 35 mol% of TANI results in an inelastic product, whilst the limitation for TANI-PB is only 1 mol% of TANI. Therefore, the increases in the relative permittivity through introducing conducting TANI groups to the polymer backbones are limited by the offset in mechanical properties and loss of elasticity.

This work successfully demonstrates the intrinsic grafting of conducting groups to the backbone of elastomers. It introduces an alternative to extrinsically mixing conducting groups to elastomers, and synthesises modified SBS and PB elastomers with enhanced electrical properties for actuation applications, such as artificial muscles and energy harvesting devices. Based on the results of this work, further work will involve the actuation testing of 1 mol% TANI-PB, 25 mol% TANI-SBS and 35 mol% TANI-SBS to establish the actuation performance and the breakdown strengths of the elastomers

Supplementary Materials: The following are available online at http://www.mdpi.com/2504-477X/4/1/25/s1, Figure S1: GPC trace from the synthesis of TANI, Figure S2: ^{1}H NMR with assigned peaks of TANI, Figure S3: FTIR of TANI, SBS and TANI-SBS with notable peaks highlighted, Figure S4: FTIR of TANI, PB and TANI-PB with notable peaks highlighted, Figure S5: ^{1}H NMR of PB, e-PB and TANI-PB with notable peaks assigned, Figure S6: DMTA of 50 mol% TANI-PB with T_g transition peaks highlighted, Figure S7: UV-Vis spectroscopy of TANI, Figure S8: GPC trace of SBS and PB, Figure S9: Stress strain curve of SBS and PB, Figure S10: (a) relative permittivity, (b) tan δ, (c) AC Conductivity and (d) phase angle for TANI in the emeraldine salt oxidation state, Figure S11: AC Conductivity of (a) SBS, 25 mol% TANI-SBS and 35 mol% TANI-SBS and (b) PB, 1 mol% TANI-PB, 25 mol% TANI-PB and 35 mol% TANI-PB.

Author Contributions: C.E., A.P. and C.W. devised the project. C.E., A.P. and A.M.W. carried out the experimentation and analysis. C.E., A.P., A.M.W. and C.W. All contributed to writing the article. All authors have read and agreed to the published version of the manuscript.

Funding: C.E. wishes to thank EPSRC and Jaguar Land Rover (UK) for funding this PhD studentship.

Conflicts of Interest: The authors declare no conflict of interest.

References

1. Stoyanov, H.; Kollosche, M.; McCarthy, D.N.; Kofod, G. Molecular composites with enhanced energy density for electroactive polymers. *J. Mater. Chem.* **2010**, *20*, 7558–7564. [CrossRef]
2. Ellingford, C.; Zhang, R.; Wemyss, A.M.; Bowen, C.; McNally, T.; Figiel, Ł.; Wan, C. Intrinsic Tuning of Poly(styrene–butadiene–styrene)-Based Self-Healing Dielectric Elastomer Actuators with Enhanced Electromechanical Properties. *ACS Appl. Mater. Interfaces* **2018**, *10*, 38438–38448. [CrossRef]
3. Minaminosono, A.; Shigemune, H.; Okuno, Y.; Katsumata, T.; Hosoya, N.; Maeda, S. A Deformable Motor Driven by Dielectric Elastomer Actuators and Flexible Mechanisms. *Front. Robot. AI* **2019**, *6*. [CrossRef]
4. Brochu, P.; Pei, Q. Advances in Dielectric Elastomers for Actuators and Artificial Muscles. *Macromol. Rapid Commun.* **2010**, *31*, 10–36. [CrossRef]
5. Kornbluh, R.D.; Pelrine, R.; Pei, Q.; Heydt, R.; Stanford, S.; Oh, S.; Eckerle, J. Electroelastomers: Applications of dielectric elastomer transducers for actuation, generation, and smart structures. In Proceedings of the SPIE's 9th Annual International Symposium on Smart Structures and Materials, San Diego, CA, USA, 9 July 2002; p. 17.
6. Laschi, C.; Mazzolai, B.; Cianchetti, M. Soft robotics: Technologies and systems pushing the boundaries of robot abilities. *Sci. Robot.* **2016**, *1*, 3690. [CrossRef]
7. Ellingford, C.; Bowen, C.; McNally, T.; Wan, C. Intrinsically Tuning the Electromechanical Properties of Elastomeric Dielectrics: A Chemistry Perspective. *Macromol. Rapid Commun.* **2018**, *39*, 1800340. [CrossRef]
8. Pelrine, R.; Kornbluh, R.; Eckerle, J.; Jeuck, P.; Oh, S.J.; Pei, Q.B.; Stanford, S. Dielectric elastomers: Generator mode fundamentals and applications. In Proceedings of the Smart Structures and Materials 2001 Conference, Newport Beach, CA, USA, 5–8 March 2001; pp. 148–156.
9. Zhang, X.; Shen, Y.; Zhang, Q.; Gu, L.; Hu, Y.; Du, J.; Lin, Y.; Nan, C.W. Ultrahigh Energy Density of Polymer Nanocomposites Containing BaTiO3@TiO2 Nanofibers by Atomic-Scale Interface Engineering. *Adv. Mater.* **2015**, *27*, 819–824. [CrossRef]
10. Madsen, F.B.; Yu, L.; Skov, A.L. Self-Healing, High-Permittivity Silicone Dielectric Elastomer. *ACS Macro Lett.* **2016**, *5*, 1196–1200. [CrossRef]

11. Zhou, J.; Jiang, L.; Khayat, R.E. Investigation on the performance of a viscoelastic dielectric elastomer membrane generator. *Soft Matter* **2015**, *11*, 2983–2992. [CrossRef]
12. Romasanta, L.J.; Lopez-Manchado, M.A.; Verdejo, R. Increasing the performance of dielectric elastomer actuators: A review from the materials perspective. *Prog. Polym. Sci.* **2015**, *51*, 188–211. [CrossRef]
13. Yuan, J. Percolation of carbon nanomaterials for high-k polymer nanocomposites. *Chin. Chem. Lett.* **2017**, *28*, 2036–2044. [CrossRef]
14. Chi, Q.G.; Dong, J.F.; Zhang, C.H.; Wong, C.P.; Wang, X.; Lei, Q.Q. Nano iron oxide-deposited calcium copper titanate/polyimide hybrid films induced by an external magnetic field: Toward a high dielectric constant and suppressed loss. *J. Mater. Chem. C* **2016**, *4*, 8179–8188. [CrossRef]
15. Yuan, J.; Yao, S.; Poulin, P. Dielectric Constant of Polymer Composites and the Routes to High-k or Low-k Nanocomposite Materials. In *Polymer Nanocomposites: Electrical and Thermal Properties*; Huang, X., Zhi, C., Eds.; Springer International Publishing: Cham, Switzerland, 2016; pp. 3–28.
16. Zhang, L.; Wang, W.; Wang, X.; Bass, P.; Cheng, Z.Y. Metal-polymer nanocomposites with high percolation threshold and high dielectric constant. *Appl. Phys. Lett.* **2013**, *103*, 232903. [CrossRef]
17. Wu, S.Q.; Wang, J.W.; Shao, J.; Wei, L.; Yang, K.; Ren, H. Building a Novel Chemically Modified Polyaniline/Thermally Reduced Graphene Oxide Hybrid through π–π Interaction for Fabricating Acrylic Resin Elastomer-Based Composites with Enhanced Dielectric Property. *ACS Appl. Mater. Interfaces* **2017**, *9*, 28887–28901. [CrossRef] [PubMed]
18. Roscow, J.I.; Bowen, C.R.; Almond, D.P. Breakdown in the Case for Materials with Giant Permittivity? *ACS Energy Lett.* **2017**, *2*, 2264–2269. [CrossRef]
19. Zhao, H.; Xia, Y.J.; Dang, Z.M.; Zha, J.W.; Hu, G.H. Composition dependence of dielectric properties, elastic modulus, and electroactivity in (carbon black-BaTiO3)/silicone rubber nanocomposites. *J. Appl. Polym. Sci.* **2013**, *127*, 4440–4445. [CrossRef]
20. Nayak, S.; Chaki, T.K.; Khastgir, D. Development of Flexible Piezoelectric Poly(dimethylsiloxane)–BaTiO3 Nanocomposites for Electrical Energy Harvesting. *Ind. Eng. Chem. Res.* **2014**, *53*, 14982–14992. [CrossRef]
21. Stoyanov, H.; Mc Carthy, D.; Kollosche, M.; Kofod, G. Dielectric properties and electric breakdown strength of a subpercolative composite of carbon black in thermoplastic copolymer. *Appl. Phys. Lett.* **2009**, *94*, 232905. [CrossRef]
22. Hwang, W.F.; Wiff, D.R.; Benner, C.L.; Helminiak, T.E. Composites on a molecular level: Phase relationships, processing, and properites. *J. Macromol. Sci. Part B* **1983**, *22*, 231–257. [CrossRef]
23. Zhao, W.; Glavas, L.; Odelius, K.; Edlund, U.; Albertsson, A.-C. A robust pathway to electrically conductive hemicellulose hydrogels with high and controllable swelling behavior. *Polymer* **2014**, *55*, 2967–2976. [CrossRef]
24. Chen, C.H. Thermal and morphological studies of chemically prepared emeraldine-base-form polyaniline powder. *J. Appl. Polym. Sci.* **2003**, *89*, 2142–2148. [CrossRef]
25. Sapurina, I.; Tenkovtsev, A.V.; Stejskal, J. Conjugated polyaniline as a result of the benzidine rearrangement. *Polym. Int.* **2015**, *64*, 453–465. [CrossRef]
26. Liu, L.; Yan, S.; Zhang, L. A Self-Healing Dielectric Supramolecular Elastomer Functionalized with Aniline Tetramer. *Macromol. Rapid Commun.* **2018**, *39*, 1800349. [CrossRef] [PubMed]
27. Lv, Q.C.; Li, Y.; Zhong, Z.K.; Wu, H.J.; He, F.A.; Lam, K.H. Preparation and dielectric properties of novel composites based on oxidized styrene-butadienestyrene copolymer and polyaniline modified exfoliated graphite nanoplates. *Appl. Surf. Sci.* **2018**, *441*, 945–954. [CrossRef]
28. Takayanagi, M. Polymer composites of rigid and flexible molecules. *Pure Appl. Chem.* **1983**, *55*, 819. [CrossRef]
29. Pohl, H.; Rosen, R. *Bull. Am. Phys. Soc.* **1965**, *10*, 396.
30. Li, C.H.; Wang, C.; Keplinger, C.; Zuo, J.L.; Jin, L.; Sun, Y.; Zheng, P.; Cao, Y.; Lissel, F.; Linder, C.; et al. A highly stretchable autonomous self-healing elastomer. *Nat. Chem.* **2016**, *8*, 618–624. [CrossRef]
31. Espino, D.; Haruvy-Manor, Y.; Mastai, Y. $CoFe_2O_4$ Nano-particles for Radical Oxidative Degradation of High Molecular Weight Polybutadiene. *J. Polym. Environ.* **2019**, *27*, 827–836. [CrossRef]
32. Mirmohammadi, S.A.; Nekoomanesh-Haghighi, M.; Mohammadian Gezaz, S.; Bahri-Laleh, N.; Atai, M. In-situ photocrosslinkable nanohybrid elastomer based on polybutadiene/polyhedral oligomeric silsesquioxane. *Mater. Sci. Eng. C* **2016**, *68*, 530–539. [CrossRef]

33. Bai, J.; Li, H.; Shi, Z.; Yin, J. An Eco-Friendly Scheme for the Cross-Linked Polybutadiene Elastomer via Thiol–Ene and Diels–Alder Click Chemistry. *Macromolecules* **2015**, *48*, 3539–3546. [CrossRef]
34. Rajabi, F.H.; Nikje, M.M.A.; Taslimipour, T. Epoxidation of Styrene–Butadiene Rubber (SBR) Using In Situ Generated Dimethyldioxirane (DMD): Characterization and Kinetic Study. *Des. Monomers Polym.* **2010**, *13*, 535–546. [CrossRef]
35. Qin, J.; Lin, F.; Hubble, D.; Wang, Y.; Li, Y.; Murphy, I.A.; Jang, S.H.; Yang, J.; Jen, A.K.Y. Tuning self-healing properties of stiff, ion-conductive polymers. *J. Mater. Chem. A* **2019**, *7*, 6773–6783. [CrossRef]
36. Wang, Z.; Lu, X.; Sun, S.; Yu, C.; Xia, H. Preparation, characterization and properties of intrinsic self-healing elastomers. *J. Mater. Chem. B* **2019**, *7*, 4876–4926. [CrossRef] [PubMed]
37. Pan, Y.; Hu, J.; Yang, Z.; Tan, L. From Fragile Plastic to Room-Temperature Self-Healing Elastomer: Tuning Quadruple Hydrogen Bonding Interaction through One-Pot Synthesis. *ACS Appl. Polym. Mater.* **2019**, *1*, 425–436. [CrossRef]
38. Guo, B.; Finne-Wistrand, A.; Albertsson, A.C. Facile Synthesis of Degradable and Electrically Conductive Polysaccharide Hydrogels. *Biomacromolecules* **2011**, *12*, 2601–2609. [CrossRef]
39. Baker, C.O.; Huang, X.; Nelson, W.; Kaner, R.B. Polyaniline nanofibers: Broadening applications for conducting polymers. *Chem. Soc. Rev.* **2017**, *46*, 1510–1525. [CrossRef]
40. Thota, A.; Arukula, R.; Narayan, R.; Sripadi, P.; Bojja, S.; Rao, C.R.K. Electrochemical Synthesis and Reduction of Aniline-Tetramer: Application Prospect as MOR Electrocatalyst. *J. Electrochem. Soc.* **2017**, *164*, 1090–1099. [CrossRef]
41. Gul, S.; Shah, A.H.A.; Bilal, S. Synthesis and Characterization of Processable Polyaniline Salts. *J. Phys. Conf. Ser.* **2013**, *439*, 012002. [CrossRef]
42. Patil, A.O.; Heeger, A.J.; Wudl, F. Optical properties of conducting polymers. *Chem. Rev.* **1988**, *88*, 183–200. [CrossRef]